Some Two-Body Final States of K^-p Interactions at 1.33 GeV/c*

W. P. TROWER,† J. R. FICENEC,† R. I. HULSIZER,§ J. LATHROP,‖ J. N. SNYDER AND W. P. SWANSON**
Department of Physics, University of Illinois, Urbana, Illinois
(Received 31 August 1967)

We studied 21 187 two-prong, two-prong-with-kink, and zero-prong-V events at incident kaon momentum of 1.33 GeV/c using the 72-in. hydrogen bubble chamber at the Lawrence Radiation Laboratory and two scanning and measuring projectors in Urbana. We determined the total and partial cross sections for all contributing reactions. For the two-body final states, some production and polarization angular distributions were measured. The angular distributions are discussed in terms of exchanges in the kinematical channels s, t, and u assuming the simplest Feynman graphs. Elastic scattering is analyzed as a diffraction process.

I. INTRODUCTION

THE general interest in the K^-p interaction, the discovery of the Kerth bump in the total K^-p cross section, and the success of the K^- exposure in the 15-in. liquid-hydrogen bubble chamber led the Alvarez group, at the Lawrence Radiation Laboratory, to propose an extensive exposure of the 72-in. liquid-hydrogen bubble chamber to K^- mesons of momenta 1–2 GeV/c. A separated beam was designed and built for this purpose.[1] As part of a general Berkeley-Illinois collaboration, we undertook the study of some of the reactions that occurred in the particular exposure where the K^- mesons had a momentum of 1.33 GeV/c.

At the outset of this experiment, data available within the incident-kaon momentum range 0.80–1.80 GeV/c consisted of determinations of the total K^-p cross sections as well as data pertaining to the two-body cross sections below 1.15 GeV/c.[2] Since that time numerous experiments have contributed data to the total and partial cross sections between 0.80 and 1.80 GeV/c.[3]

The first reaction chosen for study was K^-p elastic scattering. Since all the particles are charged, all the particle momenta can be measured, and the consistency of the measurements with momentum and energy conservation provided a check of the new measuring apparatus which had been built for the experiments. The apparatus was a scanning and measuring projector (SMP) which had been invented by L. W. Alvarez and developed as part of the collaboration.[4]

Once the measuring apparatus had been shown to produce accurate data, the rest of the two- and three-body reactions were studied. The total cross section at this momentum, partial and differential cross sections, decay angular distributions, and resonance production were studied in the reactions that produced final states of $\bar{K}N$, $\bar{K}N\pi$, $Y\pi$, Ξ^-K^+, and $Y\pi\pi$. Some of the four-body final states as well as one production topology of Ξ^-K^+ occurring in this exposure have been

* Work supported by the U. S. Atomic Energy Commission. Funds for operation of the computer provided by the NSF. Part of this work presented by W. P. T. in partial fulfillment of the requirements for the Ph.D. degree at the University of Illinois.
† Present address: Physics Department, Virginia Polytechnic Institute, Blacksburg, Va.
§ Present address: Physics Department, Massachusetts Institute of Technology, Cambridge, Mass.
‖ Present address: University of Witwatersrand, Johannesburg, Union of South Africa.
**Present address: CERN, Geneva, Switzerland.

[1] H. K. Ticho, D. H. Stork, J. Button-Schafer, G. R. Kalbfleisch, D. H. Miller, J. Kirz, R. Hubbard, D. O. Huwe, and C. G. Wohl, University of California Lawrence Radiation Laboratory Report No. UCRL-10690, 1965 (unpublished).

[2] (a) V. Cook, B. Cork, T. F. Hoang, D. Keefe, L. T. Kerth, W. A. Wenzel, and T. F. Zipf, Phys. Rev. **123**, 320 (1961); (b) O. Chamberlain, K. M. Crowe, D. Keefe, L. T. Kerth, A. Lemonick, Tin Maung, and T. F. Zipf, *ibid.* **125**, 1696 (1962); (c) P. L. Bastien and J. P. Berge, Phys. Rev. Letters **10**, 188 (1963); (d) W. Graziano and S. G. Wojcicki, Phys. Rev. **128**, 1868 (1962).

[3] (a) L. Sodickson, I. Mannelli, D. Frisch, and M. Wahlig, Phys. Rev. **133**, B757 (1964); (b) W. R. Holley, E. F. Beall, D. Keefe, J. Kerth, J. J. Thresher, C. L. Wang, and W. A. Wenzel, *ibid.* **154**, 1273 (1967); (c) C. G. Wohl, F. T. Solmitz, and M. L. Stevenson, Phys. Rev. Letters **17**, 107 (1966); (d) P. M. Dauber, *ibid.* **134**, B1370 (1964); (e) A. Barbaro-Galtieri, M. H. Alston, A. H. Rosenfeld, and S. G. Wojcicki, Bull. Am. Phys. Soc. **9**, 23 (1964); (f) B. Buschback-Czapp, I. Wacek, W. A. Cooper, A. Fridman, E. Malamud, G. Otter, E. Gelsema, and A. Tenner, in *Proceedings of the Sienna International Conference on Elementary Particles and High-Energy Physics, 1963*, edited by G. Bernardini and G. P. Puppi (Società Italiana di Fisica, Bologna, 1963), p. 166; (g) P. M. Dauber, P. E. Schlein, W. A. Slater, D. H. Stork, and H. K. Ticho, Phys. Letters **23**, 154 (1966); (h) P. E. Eberhard, S. M. Flatte, D. O. Huwe, J. Button-Schafer, F. T. Solmitz, and M. L. Stevenson, Phys. Rev. **145**, 1062 (1966); (i) P. M. Dauber, W. H. Dunwoodie, P. E. Schlein, W. E. Slater, L. T. Smith, D. H. Stork, and H. K. Ticho, in *Proceedings of the Second Topical Conference on Resonant Particles, Athens, Ohio, 1965* (Ohio University, Athens, Ohio, 1965) p. 380; (j) G. B. Yodh, *ibid.* p. 269; (k) J. P. Berge, P. Eberhard, J. R. Hubbard, D. W. Merrill, J. Button-Shafer, F. T. Solmitz, and M. L. Stevenson, Phys. Rev. **147**, 945 (1966); (l) R. Armenteros, M. Ferro-Luzzi, D. W. G. Leith, R. Levi-Setti, A. Minten, R. D. Tripp, H. Filthuth, V. Hepp, E. Kluge, H. Schneider, R. Barloutaud, P. Garnet, J. Meyer, and J. P. Porte, Phys. Letters **24B**, 198 (1967); (m) J. D. Davies, J. D. Dowell, P. M. Hattersley, R. J. Homer, A. W. O'Dell, A. A. Carter, K. F. Riley, R. J. Tapper, D. V. Bugg, R. S. Gilmore, K. M. Knight, D. C. Salter, G. H. Stafford, and E. J. N. Wilson, Phys. Rev. Letters **18**, 62 (1967); (n) R. L. Cool, G. Giacomelli, T. F. Kycia, B. A. Leontic, K. K. Li, A. Lundby, and J. Teiger, *ibid.* **16**, 1228 (1966); (o) N. M. Gelfand, D. Harmsen, R. Levi-Setti, E. Predazzi, M. Raymond, J. Doede, and W. Männer, *ibid.* **17**, 1224 (1966).

[4] P. G. Davey, R. I. Hulsizer, W. E. Humphrey, J. H. Munson, R. R. Ross, and A. J. Schwemin, Rev. Sci. Instr. **35**, 1134 (1964).

analyzed by the Alvarez group.[5] This paper reports the total and nonresonant cross sections and two-body angular distributions, and compares our results with other experiments.

II. EXPERIMENTAL PROCEDURE

A. Scanning and Measuring

The data that have been analyzed are contained on 93 rolls of 46-mm film containing about 600 sets of stereo triads each. The total exposure consisted of about 56 000 stereo triads.

For this experiment, an event was any interaction or three-prong decay which was associated with a beam track. A beam track was defined as a negatively charged particle entering the chamber between the flanges of the window and not deviating in azimuth by more than 2° from the central angle of the majority of other entering tracks. Each roll was scanned twice by different scanners. When both scans of a roll were complete, the results were collated and discrepancies were noted. Discrepant interpretations were then resolved by re-examination. The scanning efficiencies for each topology were calculated by the following prescription:

$$\text{efficiency}=\frac{N_c(N_1+N_2-N_c)}{N_1N_2}, \qquad (1)$$

where N_c is the number of events found after collation, N_1 is the number of events found on first scan, and N_2 is the number of events found on second scan. This calculation is based on the assumption that events are missed only as a result of random inefficiency. The efficiencies were 95–99% for the various topologies.

Of all the events found by scanning, the ones that were measured were the two-prong (2P), zero-prong-V (0PV), two-prong with a kink on the negative secondary ($2P^-$), and two-prong with a kink on the positive fitted secondary ($2P^+$) events. The measurements were fitted to the mass hypotheses displayed in Fig. 1.

TABLE I. Final results of the measurement effort. "Passed" means that the measurements satisfied some physical hypothesis. "Unpassed" means that the event was judged unmeasurable or yielded measurements that failed to satisfy some hypothesis after three measurements.

Topology	Passed (%)	Unpassed (%)
2P	81.0	19.0
0PV	73.7	26.3
$2P^+$	68.9	31.1
$2P^-$	71.9	28.1

[5] (a) S. G. Wojcicki, M. H. Alston, and G. R. Kalbfleisch, Phys. Rev. 135, B495 (1964); (b) L. W. Alvarez, J. P. Berge, G. R. Kalbfleisch, J. Button-Schafer, F. T. Solmitz, M. L. Stevenson, and H. K. Ticho, in *Proceedings of the 1962 Annual International Conference on High-Energy Physics at CERN*, edited by J. Prentki (CERN, Geneva, 1962), p. 433.

Events which satisfied a kinematical hypothesis to a 1% confidence level were considered to be good events. Operators were allowed to reject events without attempting a measurement, if they determined that a successful measurement would be impossible because of the quality of the film or the placement of the event. Measured events that failed to satisfy any hypothesis were remeasured. Those remeasured events that satisfied a hypothesis were classed as good; those that failed were measured a third time. After this measurement, passing events were called good, but failed events were not remeasured. These unpassed events were divided among the various hypotheses in proportion to the passed events. Table I has the final results of the measurement program.

B. Beam Characteristics

1. Momentum

We used two methods to establish the beam momentum. First, 527 two-prong events, whose measurements fit some definite mass hypothesis and which had a beam track longer than 15 cm were used. The unfitted momentum of the beam track was extrapolated to the middle of the chamber, and the set of values were fitted to a Gaussian distribution. These data and the fitted curve are displayed in Fig. 2(a). In the second determination, 158 events were selected, whose measurements fit the mass hypothesis of the τ-decay mode of the K^- meson. For each selected event, the fitted kaon momentum was extrapolated to the middle of the chamber. The data and a Gaussian distribution fitted to the data are shown in Fig. 2(b). The weighted average of the two determinations is $P_{\text{beam}}=1.328\pm0.002$ GeV/c and $\Delta P_{\text{beam}}=0.036\pm0.002$ GeV/c.

2. Path Length

To determine the path length of beam tracks in the interaction volume, we counted the number of entering beam tracks N_B and determined a value for the average path length in the chamber. Rather than measuring a randomly selected set of noninteracting beam tracks for this, we extrapolated each interacting beam track that produced a good event to its intersections with the interaction volume, weighted each track by the reciprocal of its length, and averaged the weighted lengths.[6] This gave an average path length of

$$\bar{l}=155.9\pm1.6 \text{ cm}.$$

The total path length was

$$L=N_B\bar{l}=(1.12\pm0.02)\times10^7 \text{ cm}.$$

[6] The probability that a beam particle would have an interaction is proportional to its length, so the weight given the extrapolated length of each interacting beam track was the reciprocal of its length.

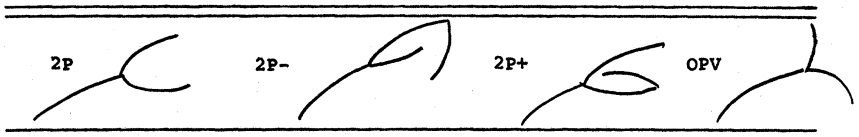

$K^-p \to K^-p$	$K^-p \to \Sigma^-\pi^+$	$K^-p \to \Sigma^+(n)\pi^-$	$K^-p \to \Lambda\,\pi^\circ$
$K^-p\pi^\circ$	$\Sigma^-\pi^+\pi^\circ$	$\Sigma^+(p)\pi^-$	Λ mm
K^-p mm	$\Sigma^-\pi^+$ mm	$\Sigma^+(n)\pi^-\pi^\circ$	$\bar{K}^\circ$ n
$K^-\pi^+n$	K^-p	$\Sigma^+(n)\pi^-$ mm	$\bar{K}^\circ$ mm
$K^-\pi^+$ mm	$K^-p\,\pi^\circ$	$\Sigma^+(p)\pi^-\pi^\circ$	
$\pi^-p\,\bar{K}^\circ$	K^-p mm	$\Sigma^+(p)\pi^-$ mm	
π^-p mm	$K^-\pi^+n$		
$\pi^-\pi^+\Lambda$	$K^-\pi^+$ mm		
$\pi^-\pi^+\Sigma^\circ$	Ξ^-K^+		
$\pi^-\pi^+$ mm			

FIG. 1. Kinematical mass hypotheses attempted for each topology. Note that mm is just some missing mass and the baryon involved in the decay for the Σ^+ is indicated in the brackets.

3. *Beam Contamination*

The beam was known from other studies[7] to consist mainly of kaons, but to have some contamination of pions and muons. No electrons were expected in the beam since they would suffer a 500-MeV energy loss in the 0.25-in. stainless-steel entrance window of the chamber.[8] Their radius of curvature would thus be easily distinguishable from that of the acceptable beam tracks. The contamination of pions was estimated to be less than 3% because no example of pion-produced associated production of strange particles was seen. A more restrictive estimate was obtained by examining the δ rays produced by beam particles. Ten beam particles with δ rays of larger energy than can be

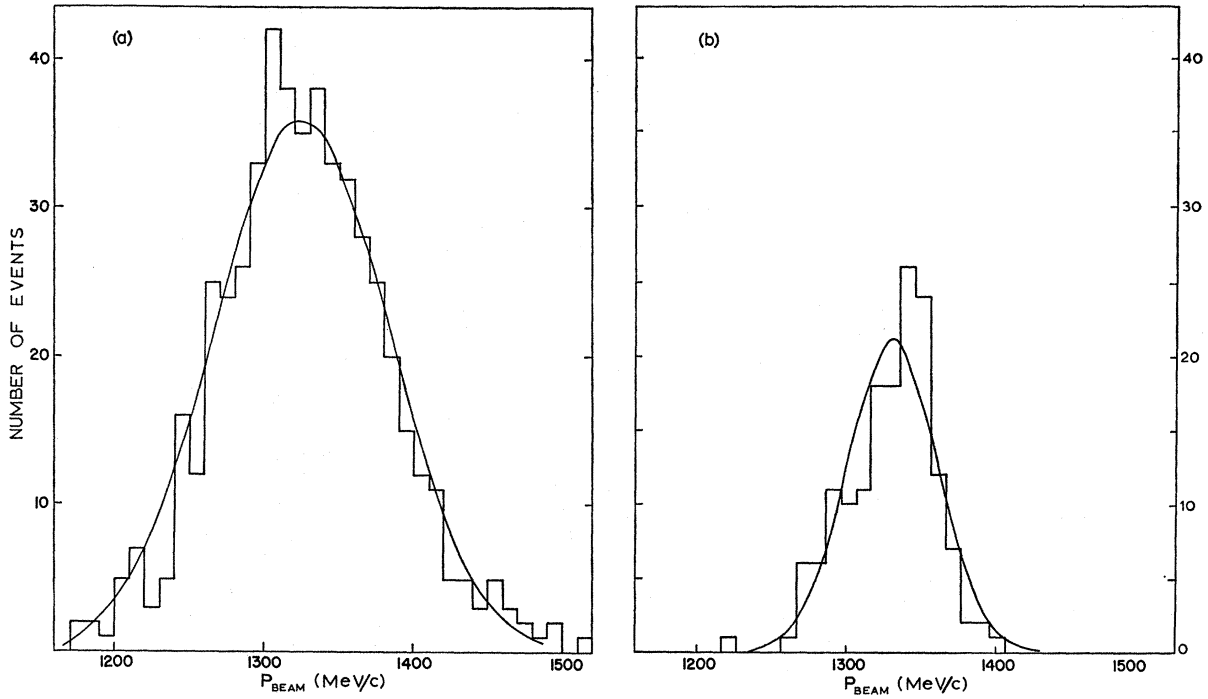

FIG. 2. Beam momentum: (a) determined by unfitted momentum measurements of the beam track from 2P events; (b) determined by measurement of τ decays.

[7] R. Hubbard, Alvarez Group Physics Note 496, 1964 (unpublished).
[8] W. P. Trower, University of California Lawrence Radiation Laboratory Report No. UCRL-2426, Vol. IV, 1965 (unpublished).

produced by a kaon at 1.33 GeV/c were subsequently seen to undergo strong interactions. This number implies that the fractional-pion contamination in the beam is $f_\pi=(1.4\pm0.5)\%$. If the rest of the beam tracks that produce δ rays of larger energy than can be produced by 1.33 GeV/c kaons are muon tracks, then the fractional-muon contamination in the beam is $f_\mu=5.1\pm1.0\%$.

C. Detection and Measurement Biases

In the determination of cross sections and angular distributions, corrections had to be made for biases in the detection and measurement of events. Each correction will be discussed in turn.

1. *Scanning Losses for Small-Angle Elastic Scattering*

Small-angle elastic scattering events are hard to see, particularly if the plane of the scattering is nearly vertical in the bubble chamber. The scattering seen by the scanner is, of course, only the projection of the true scattering on the film plane of the camera view in which the scan is done. The smallest value of the scattering angle in the film plane that could be reliably noticed by the scanners was about 11°. In addition to the small scattering angles being hard to see, the proton range becomes short, and its direction becomes transverse to the beam particle. In this bubble chamber the back plate has transverse lines on it, against which short transverse tracks are hard to see.

In order to estimate the number of elastic scattering events missed, the following argument was used: The observed angular distribution, as seen in Fig. 11, in the region $0.3\leq\cos\theta_P\leq0.925$ is fitted very well by the function $N(\theta)=\exp[-k(1-\cos\theta_P)]$. We assumed that the true distribution is represented in the region $0.925\leq\cos\theta_P\leq1.0$ by the extrapolation of this function.

2. *Distortion of Azimuthal Angular Distributions*

A disturbing and uncorrected effect is that the distribution of elastic scattering events with respect to the angle between the scattering plane and the horizontal plane in the bubble chamber is not uniform. The observed distribution is shown in Fig. 3 for those events for which $-1.0\leq\cos\theta_P<0.925$. We expect the scanning efficiency for events in this range to be high, since the range of the proton exceeds 8.2 cm. An inability to measure successfully steeply dipping tracks could account for this effect, but no disproportionate number of steeply dipping tracks was found among the unpassed events. In fact, all of the unfitted two-prong events could be accounted for as due to pions in the beam, or as due to other event types which appeared to be two-prong events, such as prompt decays of strange particles. We therefore believe that the number of two-prong events is correct, but that the azimuthal distribution has been distorted. The most likely cause of the distortion is an error in the spatial reconstruction of events from the stereo camera views. The error most probably came from a translational error in the fiducial coordinates in one of the stereo views. It was not possible to go back and check the coordinates after the distortion was found, because the bubble chamber had been taken apart and reassembled by then.

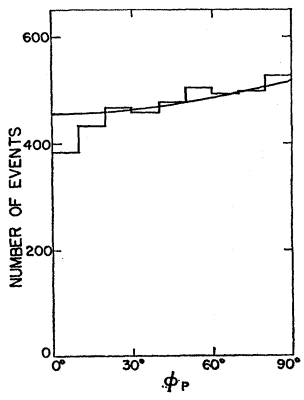

FIG. 3. Azimuthal distribution for elastic scatters in the interval $-1.00\leq\cos\theta_p<0.925$. The solid line is a best-fitted curve to the folded distribution.

The azimuthal distributions of the production and decay of the other two-body final states exhibit the same effect.

3. *Effect of Prompt, Slow, and Neutral Decays*

When an unstable particle is produced at a vertex and decays promptly, it can cause one kind of event to look like some other kind. If it decays by a neutral mode, or decays after it leaves the chamber, the decay scheme is unavailable as an identifying characteristic. The particle may then be improperly identified, and the event improperly classified. The probability of such prompt, slow, and neutral decays can be computed from the known lifetimes and branching ratios of the particles. By using the number of events with unstable particles which are found in their identifiable topologies, it is possible to estimate the number of such events which appear in other topologies as a result of these misleading decays.

The effects of these prompt, slow, and neutral decays will be to produce a contaminant in the 2P or 0PV topologies. Using a Monte Carlo calculation, their effects on the two-prong hypotheses were calculated. They contributed to the $\bar{K}^0p\pi^-$, $\Lambda^0\pi^+\pi^-$, and $\Sigma^0\pi^+\pi^-$ hypotheses to a small degree and to the $\pi^+\pi^-$ missing mass (mm) to a greater extent. Those effects were also considered when calculating the partial cross sections. Other events that manifest themselves as 0PV (K^0 decay) and $2P^+$ and $2P^-$ (pion decays) have probabilities of occurring which are small enough to justify neglecting them.

4. *Effect of Dalitz Pairs*

Reactions that usually appear as 2P, 0PV, $2P^+$, and $2P^-$ and produce a neutral pion, may appear as 4P,

2PV, 4P$^+$, and 4P$^-$, respectively. This is due to the Dalitz decay mode of the neutral pion $\pi^0 \to e^+e^-\gamma$. Since the branching to this mode is 1.18%,[9] and the number of events of a topology that fit each mass hypothesis is known, the number of events which appear in the latter set of topologies can be calculated.

5. *Detection Biases in Decays*

If we consider the decay angular distribution, defined as a function of $\cos\theta_D$ in the c.m. system of decaying particles, where

$$\cos\theta_D = \hat{P}_{\text{hyperon}} \cdot \hat{P}_{\text{baryon}} \text{ or } \hat{P}_{\bar{K}^0} \cdot \hat{P}_{\pi^+}, \quad (2)$$

we expect isotropy for the K_1^0 decay because spinless particles have no direction in space with respect to which their decay is oriented. Spin-$\frac{1}{2}$ particles in strong interactions, even with their known decay asymmetries, are also isotropic in $\cos\theta_D$ because an up-down asymmetry with respect to the production plane is averaged out by the isotropy in the distribution of the production plane itself. Therefore, any anisotropy in $\cos\theta_D$ is indicative of a bias in the data. The effect of such biases on the two reactions in which it was found is as follows.

For the $K_1^0 n$ final state, the $\cos\theta_D$ distribution is given in Fig. 4(b). Note that the two most forward bins show a marked abundance of events. We believe that this peak is due to Λ events which are kinematically ambiguous with $K_1^0 n$ events. The number of events for which the $K_1^0 n$ hypothesis is best, but which were also good fits to the Λ hypothesis, is about equal to the excess in the histogram in Fig. 4(b). To examine this excess, a scatter plot of $\cos\theta_P$ (production cosine of meson in the over-all c.m. frame) versus $\cos\theta_D$ for all ambiguous events fell in the $\cos\theta_D$ region under question. Therefore, all ambiguous events were assigned to the Λ hypothesis. The validity of this procedure was checked by a Monte Carlo calculation and found to be reasonable.

The protonic decay mode of the Σ^+ in the $\Sigma^+(p)\pi^-$ final state showed depletions in the $\cos\theta_D$ distributions near $\theta_P = +1$ and -1. We believe this to have been caused by the scanners being unable to detect small kinks in tracks in which there is little change in ionization. Therefore, only $\Sigma^+(n)\pi^-$ events weighted by their branching ratio were used in the determination of the production angular distribution and partial cross section. However, the polarization measurement is unaffected by this bias, and so the up-down decay asymmetry could be calculated for all strange-particle final states.

III. EXPERIMENTAL RESULTS

A. Total K^-p Cross Section

The total cross section was found by counting the total number of interactions, and dividing by the total path length of K mesons within the fiducial volume of the chamber. The cross section was then calculated from this ratio and from the density and atomic weight of liquid hydrogen. More precisely, the depletion of beam particles in an element of path length dl, due to interactions and decays, is

$$dN_I = (N_K \Lambda_I \exp[-l(\Lambda_D+\Lambda_I)] + N_\pi \lambda_I \exp[-l(\lambda_D+\lambda_I)])dl. \quad (3)$$

Integrating, we get

$$N_I = [N_K \Lambda_I/(\Lambda_I+\Lambda_D)](1-\exp[-\bar{l}(\Lambda_I+\Lambda_D)]) + [N_\pi \lambda_I/(\lambda_I+\lambda_D)](1-\exp[-\bar{l}(\lambda_I+\lambda_D)]). \quad (4)$$

Table II gives the values of quantities used in solving Eq. (4) for Λ_I. The result is

$$\Lambda_I = (1.069 \pm 0.028) \times 10^{-3} \text{ cm}^{-1},$$

and therefore

$$\sigma_{\text{tot}} = \Lambda_I A/N\rho = 30.5 \pm 0.8 \text{ mb}.$$

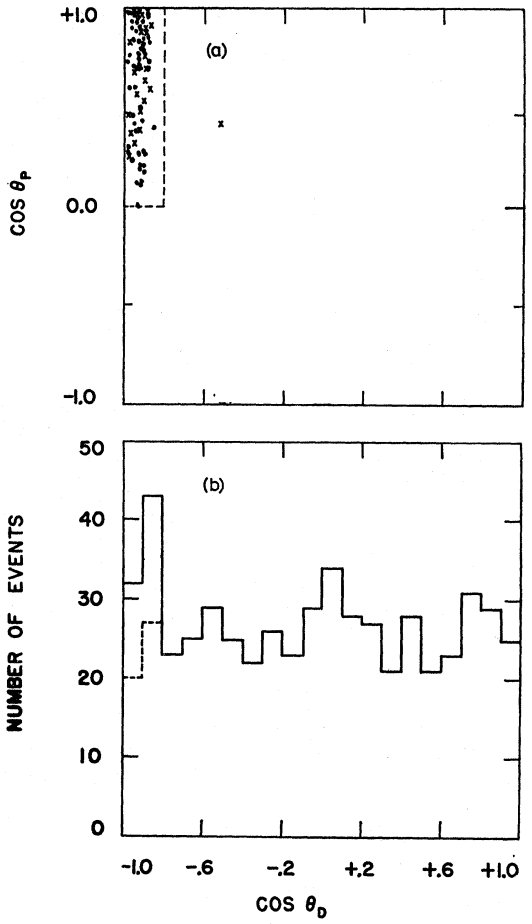

FIG. 4. (a) Scatter plot of ambiguous K_1^0 and Λ events. ● Λ, best; ×, K_1^0 best. (b) Decay angular distributions for $\bar{K}^0$ best. Solid line, uncorrected (544 events); dashed line, corrected (516 events).

[9] D. W. Joseph, Nuovo Cimento 16, 997 (1960), calculates theoretically the $\pi^0 \to e^+e^-$/anything to be 1/84.5.

TABLE II. Quantities used in calculating the total cross section.

Symbol	Quantity	Value
A	Atomic weight of hydrogen[a]	1.0084 amu
c	Speed of light[a]	2.997925×10^{10} cm/sec
f_K	Kaon beam fraction	0.935 ± 0.014
f_μ	Muon beam fraction	0.051 ± 0.018
f_π	Pion beam fraction	0.014 ± 0.005
l	Average track length	155.9 ± 1.6 cm
M_K	Kaon mass[b]	493.78 ± 0.017 MeV
M_π	Pion mass[b]	139.580 ± 0.0019MeV
N	Avagadro's number[a]	6.02252×10^{23}
N_B	No. of beam tracks	$71\,746\pm746$
N_I	No. of interactions	9747 ± 147
N_3	No. of three-prong events	518 ± 23
$N_K=f_KN_B$	No. of kaons entering chamber	$67\,227\pm1210$
$N_\pi=f_\pi N_B$	No. of pions entering chamber	1004 ± 180
P	Beam momentum	1.328 ± 0.002 GeV/c
$\Lambda_3=R_3\Lambda_D$	Inverse three-prong kaon-decay length	$(5.981\pm0.167)\times10^{-5}$ cm^{-1}
$\Lambda_D=M_K/Pc\tau_K$	Inverse kaon-decay length	$(1.0093\pm0.0272)\times10^{-3}$ cm^{-1}
$\lambda_D=M_\pi/Pc\tau_\pi$	Inverse pion-decay length	$(1.3743\pm0.0371)\times10^{-4}$ cm^{-1}
$\lambda_I=N\rho\sigma_\pi/A$	Inverse pion-interaction length	$(1.2595\pm0.0506)\times10^{-3}$ cm^{-1}
ρ	Density of liquid hydrogen[b]	0.0586 ± 0.0012 g/cm^3
σ_π	Pion total cross section[c]	35.84 ± 1.22 mb
τ_K	Kaon mean life[b]	$(1.229\pm0.008)\times10^{-8}$ sec
τ_π	Pion mean life[b]	$(2.55\pm0.0019)\times10^{-8}$ sec

[a] *Handbook of Chemistry and Physics* (Chemical Rubber Publishing Co., Cleveland, Ohio, 1965), 46th ed.
[b] See Ref. 17.
[c] See Ref. 10.

It is possible to estimate the total cross section by observing how many fewer K^- meson decays occur in the chamber than would have occurred if the K^- mesons did not interact. The value obtained by this method is

$$\sigma_{\text{tot}}(\tau \text{ decay})=43\pm18 \text{ mb}.$$

B. Classification of Events

To determine the partial cross sections and angular distributions of the various final states, it is necessary to assign each event to one of the possible final states. The fraction of events that were probably produced by π mesons must be estimated. Some events that have ambiguous identifications on the basis of track measurements can be identified by the ionization density of their tracks. The remaining ambiguous events have to be apportioned to the various final-state classifications on some probabilistic basis.

1. Subtraction of Pion-Produced Events

The total, partial, and differential cross sections of pions near our energy are well known.[10] From these and the known beam contamination due to pions, we calculated the expected number of pion-produced events in our various topologies. The probability of a pion-produced 2P$^+$ is vanishingly small. Kinematically, the pion events in the 0PV and 2P$^-$ topologies have a very small probability of fitting a kaon hypothesis and therefore will not be mistaken for kaon events. The inelastic pion events of the two-prong topology may fit some inelastic kaon hypotheses. To investigate this possibility, a Monte Carlo method was used to generate fake pion events which were tested against the set of two-prong kaon hypotheses.[11] Only the inelastic pion reaction $\pi^-p\rightarrow\pi^+\pi^-n$ makes a sizable contribution, and then only to the kaon-produced final states involving a Λ. These contributions were considered when calculating the cross sections.

In order to investigate the contributions of elastically scattered pions, we generated 915 fake events according to the known pion-production angular distribution. These events were tested against the set of kaon-mass hypotheses. The only hypothesis which they fit was kaon-proton elastic scattering with $\cos\theta_P>0.6$, where the c.m. scattering angle is

$$\cos\theta_P\equiv\hat{P}_{K_{\text{in}}}\cdot\hat{P}_{\text{meson}_{\text{out}}} \qquad (5)$$

and the $\hat{P}$'s are unit momentum vectors in the over-all c.m. system. Eighty percent of elastically scattered pions would have $\cos\theta_P>+0.6$ and 64% fit the kaon-proton elastic scattering hypothesis. A correction proportional to the number of measured events and the known pion contamination was applied to each histogram bin with $\cos\theta_P>+0.6$. This correction seemed reasonable because both the kaon- and pion-production angular distributions have similar diffraction peaks in this region.

[10] (a) W. D. Shephard and W. D. Walker, Phys. Rev. **126**, 128 (1962); (b) T. J. Devlin, B. J. Moyer, and V. Perez-Mendez, *ibid.* **125**, 690 (1962); (c) J. A. Helland, T. J. Devlin, D. E. Hagge, M. J. Longo, B. J. Moyer, and C. D. Wood, in *Proceedings of the 1962 Annual International Conference on High-Energy Physics at CERN* (CERN, Geneva, 1962), p. 3; (d) L. Bertanza, R. Carrara, A. Drago, P. Franazini, I. Mannelli, G. V. Silvestrini, and P. H. Stoker, Nuovo Cimento **19**, 467 (1961).

[11] G. R. Lynch, University of California Lawrence Radiation Laboratory Report No. UCRL-10335, 1962 (unpublished).

2. *Separation of Events by Hypothesis Testing and Ionization Measurement*

In order to associate an event with a particular physical process the confidence levels of each fitted hypothesis were compared.[12] It is well known that although χ^2 distributions of fitted bubble-chamber events exhibit the proper shape, they tend to be two- to three-times wider than those of the standard distributions. This effect is believed to be caused by an underestimation of, and/or the non-Gaussian character of, the errors in the hardware of the data-gathering system. If this effect is caused by underestimation, multiplying each calculated χ^2 by a simple scale factor will correct the situation, and in turn flatten the confidence-level distribution. To determine the scale factor, we examined about 250 measurements of events which fit a single mass interpretation for each constraint class.[13] The scale factor was found for each constraint class. When the factor was applied, the confidence-level distributions flattened out. This value for the scale factor implies an underestimation of the errors by a factor of 1.3.

An additional idea of the magnitude of the error underestimation can be obtained by examining the distributions of the pull or stretch quantities,

$$P_i(x^a)=\langle(x_i{}^a-x_i)\rangle/\langle(x_i{}^a-x_i)^2\rangle^{1/2}, \quad (6)$$

where $x_i{}^a$ is the value to which the measured variable x_i has to be adjusted in order to obtain a fit of the data to the constraints. The pull distribution should have a mean at zero and a standard deviation of unity if the errors are estimated correctly. In all of the plotted distributions, the means were consistent with zero while the widths were about 1.3–1.4, indicating an underestimation of errors of this factor.

For each event the hypothesis with the largest scaled confidence level is called "best," and, in those cases where there are ambiguities, the one with the next largest is called "next."

An event-satifying hypothesis i was judged to be ambiguous if, for any other hypothesis j, the confidence level C_j was

$$0.1C_{\text{best}}\leq C_j\leq C_{\text{best}} \quad (7)$$

and the mass assignment of one or more of the charged tracks was different from "best." For each track, projected bubble density can be predicted:

$$D\alpha 1/\beta^2\cos\lambda, \quad (8)$$

where λ is the dip of the track and $\beta=v/c$. If for those tracks (i) of the competing hypothesis (k) which have different mass assignments, the inequality

$$0.67\leq(D_{\text{best}}/D_k)_i\leq 1.5 \quad (9)$$

is unsatisfied, the ambituity is said to be resolvable by ionization examination.

All passed events that were ambiguous and were predicted to be resolvable on the basis of bubble density were examined on the scanning table to determine if the relative ionization of their tracks could specify the interaction. The success of these attempts is displayed in Table III.

TABLE III. Results of the ionization scan.

	2P	0PV	2P+	2P−
Before scan				
Unambiguous	64%	89%	79%	74%
Ambiguous	36%	11%	21%	26%
After scan				
Unambiguous	97%	95%	93%	85%
Ambiguous	3%	5%	7%	15%

After the ionization information had been used to reduce the number of ambiguous events, the classification of events was in the state shown in Table IV. In the 2P events the ambiguities are relatively few, the worst cases being those for which the choice between $K^-\pi^+n$ and $\Lambda\pi^+\pi^-$ hypotheses was ambiguous.

To identify an event with a final state having one or more neutral particles that do not decay or interact in the chamber, the mass of the missing particle must be inferred from the momentum measurements of the visible particles and the conservation laws. If only one neutral particle is actually missing, then the inferred mass may agree with that of a known particle, and the assignment is simple. If the errors are such that the mass identification is ambiguous, or if there are two unseen particles in the final state, the missing mass is calculated and the events are assigned to the possible final states in proportion to the available phase space.

The missing-mass-squared (mm^2) distribution for those events that best fit various two-body hypotheses involving neutral particles are shown in Figs. 5 and 6. The hypotheses that represent the "best" fits are (Fig. 5) $K^-p\rightarrow\bar{K}^0+$mm and (Fig. 6) $K^-p\rightarrow\Lambda+$mm. For the events that best fit $\bar{K}^0+$mm, the neutron peak is clear, and no structure appears in the remaining events. In the mm distribution for events associated with Λ production, the missing neutral can be π^0, $2\pi^0$, $3\pi^0$, η, ω, and Σ^0. The contribution of the phase-space distributions for each of these possibilities was adjusted to give the best combined fit to the observed over-all distribution. The assignments of events involving neutral particles to the other appropriate channels were made using similar decompositions.

C. Partial Cross Sections

Partial cross sections displayed in Table V were then calculated directly from the relative abundances of fitted events, with the following exceptions:

The $\Lambda\pi^0$ cross section was determined by doubling the number of 0PV events which fit the hypothesis $\Lambda+$mm

[12] H. D. Brunk, *An Introduction to Mathematical Statistics* (Ginn and Co., Boston, 1960), p. 380.

[13] J. Button-Schafer and A. H. Rosenfeld, Alvarez Group Physics Memo No. 240, 1960 (unpublished).

TABLE IV. Matrices of hypotheses fits. Abundances are given in percent of all events found in that topology. Unambigious events are diagonal terms. $\Lambda\pi^0$(lo) means that the calculated π^0 mass was less than 135 MeV.

Best / Next	2P K^-p	$K^-p\pi^0$	K^-p mm	$K^-\pi^+n$	$K^-\pi^+$ mm	$\pi^-p\bar{K}^0$	π^-p mm	$\pi^-\pi^+\Lambda$	$\pi^-\pi^+\Sigma^0$	$\pi^-\pi^+$ mm
K^-p	56.1			0.02						
$K^-p\pi^0$		7.8				0.05				
K^-p mm			0.5				0.05			
$K^-\pi^+n$	0.05			9.4				0.9	0.2	0.1
$K^-\pi^+$+mm	0.05				0.5				0.1	0.2
$\pi^-p\bar{K}^0$		0.1				7.1		0.02		
π^-p+mm	0.1	0.02	0.02				0.5		0.02	0.05
$\pi^-\pi^+\Lambda$	0.02			1.3			0.02	5.7		
$\pi^-\pi^+\Sigma^0$				0.02		0.02			3.5	
$\pi^-\pi^+$+mm	0.05	0.02		0.3	0.05	0.05				5.4

Best / Next	0PV $\Lambda\pi^0$(lo)	$\Lambda\pi^0$(hi)	Λ+mm	$\bar{K}^0n^0$	$\bar{K}^0$+mm
$\Lambda\pi^0$(lo)	9.6			0.1	
$\Lambda\pi^0$(hi)		16.9		0.1	0.003
Λ+mm			33.7	0.8	0.003
$\bar{K}^0n$	0.4	0.8	1.1	18.5	
$\bar{K}^0$ mm	0.03	0.3	1.4		16.3

Best / Next	2P+ $\Sigma^+(n)\pi^-$	$\Sigma^+(p)\pi^-$	$\Sigma^+(n)\pi^-\pi^0$	$\Sigma^+(p)\pi^-\pi^0$	$\Sigma^+(n)\pi^-$ +mm	$\Sigma^+(p)\pi^-$ +mm
$\Sigma^+(n)\pi^-$	25.4	0.1	0.9		0.06	
$\Sigma^+(p)\pi^-$	0.06	17.9				
$\Sigma^+(n)\pi^-\pi^0$	1.8		25.9			
$\Sigma^+(p)\pi^-\pi^0$		1.0	0.2	18.2		
$\Sigma^+(n)\pi^-$+mm	0.8	0.3	0.3	0.2	2.3	
$\Sigma^+(p)\pi^-$+mm	0.06	0.8	0.3		0.06	3.4

Best / Next	2P− $\Sigma^-(n)\pi^+$	$\Sigma^-(n)\pi^+\pi^0$	$\Sigma^-(n)\pi^+$+mm	K^-p	$K^-p\pi^0$	K^-p+mm	$K^-\pi^+n$	$K^-\pi^+$+mm	$K^+\Xi^-$
$\Sigma^-(n)\pi^+$	19.8	0.3	0.05	0.05	0.1	0.05			
$\Sigma^-(n)\pi^+\pi^0$	1.4	33.9			0.5		3.9		0.1
$\Sigma^-(n)\pi^+$+mm	0.6		2.2	0.1	0.1		0.7		0.1
K^-p	0.1			15.0					
$K^-p\pi^0$	0.2	0.05		0.4	5.2				0.05
K^-p+mm	0.05					0.6	0.2		
$K^-\pi^+n$	0.1	5.0	0.1				6.8		0.05
$K^-\pi^+$+mm		0.5	0.05					0.5	
$K^+\Xi^-$		0.1							0.8

with mm$\leq$135 MeV. The justification for this is that these events form a relatively pure sample of $\Lambda\pi^0$ events, whereas Λ+mm with mm>135 MeV contain $\Sigma^0\pi^0$, as well as three-body final states. In addition, the $\Lambda\pi^0$, peak, even if not truly Gaussian, should at least be symmetric about the mm$=M_{\pi^0}$.

The partial cross section for the reaction $K^-p\rightarrow\Sigma^0\pi^0$ was calculated by

$$\sigma_{\Sigma^0\pi^0}=\frac{\%(\rightarrow\Sigma^0\pi^0)}{\%(\rightarrow\Lambda\pi^0)}\sigma_{\Lambda\pi^0}, \tag{10}$$

TABLE V. Some partial cross sections in mb of K^-p reactions at 1.33 GeV/c.

Two-body final states	Three-body final states	Final states with more than one missing neutral
		$m\geq1$
$\sigma_{K^-p}=9.74\pm0.30$	$\sigma_{K^-p\pi^0}=1.30\pm0.08$	$\sigma_{\pi^-\pi^+(\Lambda,\Sigma^0)m\pi^0}=1.50\pm0.35$
$\sigma_{\bar{K}^0n}=1.78\pm0.17$	$\sigma_{K^-n\pi^+}=1.82\pm0.12$	$\sigma_{K^-\pi^+nm\pi^0}=0.09\pm0.02$
$\sigma_{\Sigma^+\pi^-}=1.48\pm0.15$	$\sigma_{\bar{K}^0p\pi^-}=1.51\pm0.11$	$\sigma_{\pi^-p\bar{K}^0m\pi^0}=0.08\pm0.03$
$\sigma_{\Sigma^-\pi^+}=0.49\pm0.03$	$\sigma_{\Sigma^+\pi^-\pi^0}=1.33\pm0.19$	$\sigma_{\bar{K}^0nm\pi^0}=1.62\pm0.19$
$\sigma_{\Sigma^0\pi^0}=0.75\pm0.12$	$\sigma_{\Sigma^-\pi^+\pi^0}=0.86\pm0.12$	$m\geq2$
$\sigma_{\Lambda\pi^0}=1.12\pm0.14$	$\sigma_{\Lambda\pi^+\pi^-}=2.48\pm0.25$	$\sigma_{K^-pm\pi^0}=0.10\pm0.02$
$\sigma_{\Delta\eta}=0.23\pm0.05$	$\sigma_{\Sigma^0\pi^+\pi^-}=1.30\pm0.40$	$\sigma_{\Sigma^+\pi^-m\pi^0}=0.07\pm0.03$
$\sigma_{\Xi^-K^+}=0.11\pm0.05$		$\sigma_{\Sigma^-\pi^+m\pi^0}=0.04\pm0.02$
		$\sigma_{\Lambda m\pi^0}+\sigma_{\Sigma^0m\pi^0}=1.15\pm0.18$

and for the reaction $K^-p\rightarrow\Lambda\eta$ by

$$\sigma_{\Lambda\eta}=\frac{\%(\rightarrow\Lambda\eta)}{\%(\rightarrow\Lambda\pi^0)}\sigma_{\Lambda\pi^0}, \tag{11}$$

where percentages are determined from the mm decomposition, and are shown in Fig. 6.

The $\Sigma^+\pi^-$ cross section was calculated by dividing the $\Sigma^+(n)\pi^-$ cross section by the known Σ^+ branching ratio.

The errors reflect the statistical uncertainties, the uncertainty in σ_{tot}, and the possible misidentification of events.

Note that the limits on the $\sigma_{\Sigma^0\pi^0}$ calculated by the triangle inequality,[14]

$$\{\tfrac{1}{2}[(\sigma_{\Sigma^+\pi^-})^{1/2}-(\sigma_{\Sigma^-\pi^+})^{1/2}]\}^2\leq\sigma_{\Sigma^0\pi^0}\leq\{\tfrac{1}{2}[(\sigma_{\Sigma^+\pi^-})^{1/2}+(\sigma_{\Sigma^-\pi^+})^{1/2}]\}^2, \tag{12}$$

are $0.07\leq\sigma_{\Sigma^0\pi^0}\leq0.92$ mb, and bracket the value we found by decomposition.

[14] R. Levi-Setti, *Elementary Particles* (The University of Chicago Press, Chicago, 1963), Part I, p. 47.

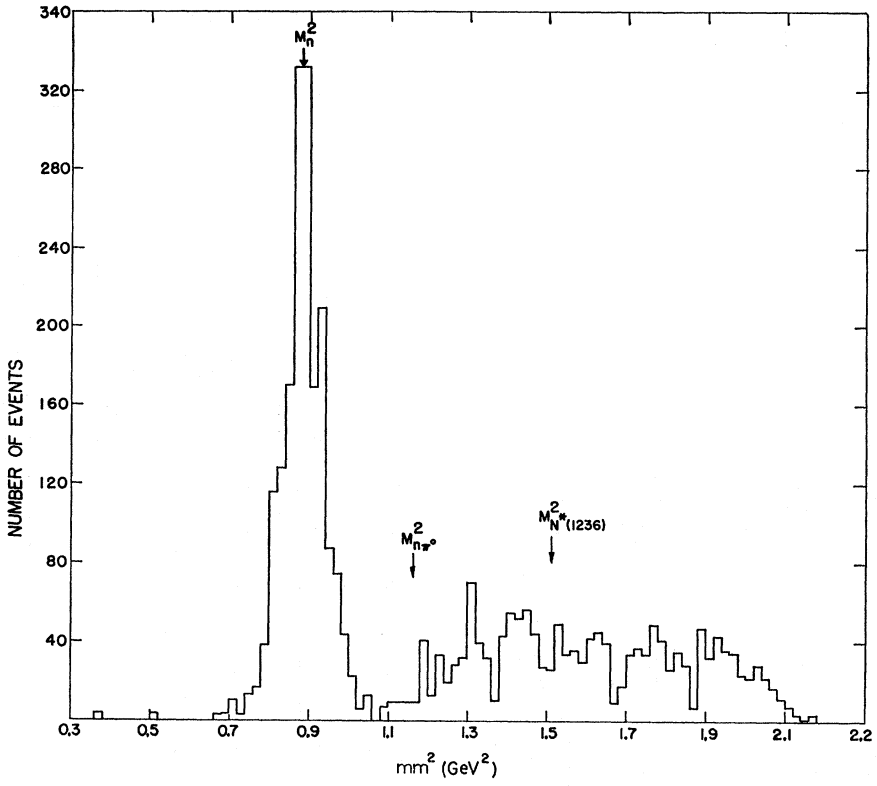

FIG. 5. Missing-mass-squared spectrum associated with K_1^0 production in the reaction $K^-p \to \bar{K}^0$ mm.

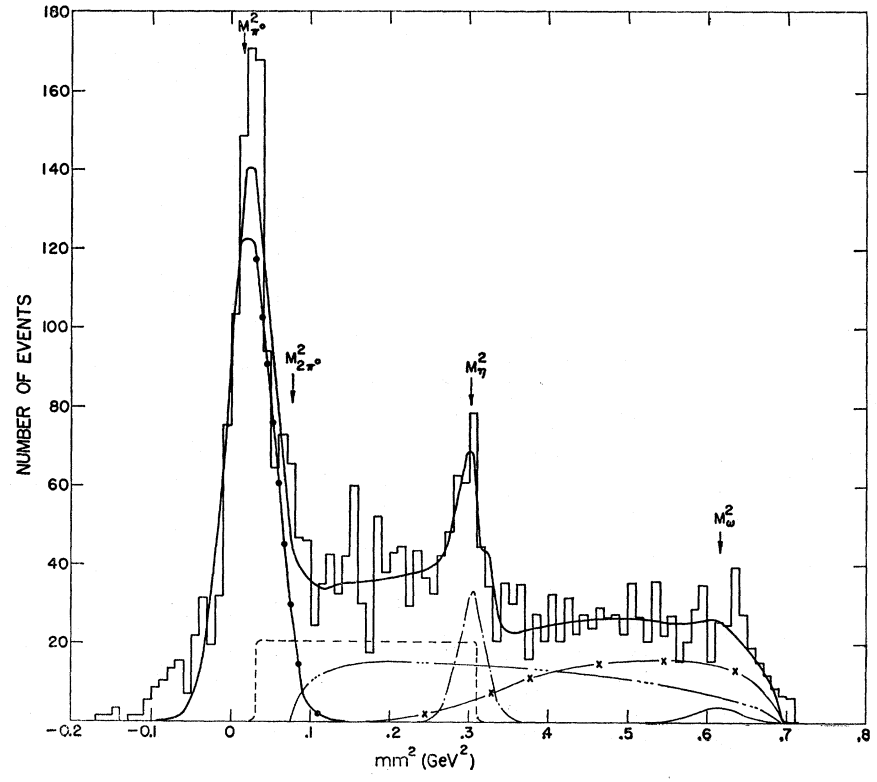

FIG. 6. Missing-mass-squared spectrum associated with Λ production in the reaction $K^-p \to \Lambda$ mm. Heavy curve, final composite curve; —●—●—, (31%) $\Lambda\pi^0$ contribution; — — —, (21%) $\Sigma^0\pi^0$ contribution; —·—, (4%) $\Lambda\eta$ contribution; ———, (1%) $\Lambda\omega$ contribution; —···—, (25%) three-body-phase-space contribution; and —×— (17%) four-body-phase-space contribution.

TABLE VI. Some two-body production angular distributions.

$K^-p \to K^-p$ Raw	Correct	Error	$\cos\theta_p$		$K^-p \to \bar{K}^0n$ Raw	Correct	Error
11	12.6	3.8	−1.00 to	−0.975	58	277.8	36.5
17	19.5	4.7	−0.975	−0.95			
28	32.1	6.1	−0.95	−0.925	30	137.2	25.1
29	33.2	6.2	−0.925	−0.90			
36	41.2	6.9	−0.90	−0.875	22	97.7	20.8
40	45.8	7.2	−0.875	−0.85			
45	51.5	7.7	−0.85	−0.825	16	69.3	17.3
38	43.5	7.1	−0.825	−0.80			
35	40.1	6.8	−0.80	−0.775	9	38.3	12.8
38	43.5	7.1	−0.775	−0.75			
36	41.2	6.9	−0.75	−0.725	6	25.2	10.3
26	29.8	5.8	−0.725	−0.70			
27	30.9	5.9	−0.70	−0.675	5	20.9	9.4
36	41.2	6.9	−0.675	−0.65			
26	29.8	5.8	−0.65	−0.625	9	37.2	12.4
31	35.5	6.4	−0.625	−0.60			
29	33.2	6.2	−0.60	−0.575	7	28.7	10.8
21	24.0	5.2	−0.575	−0.55			
25	28.6	5.7	−0.55	−0.525	13	53.5	14.9
20	22.9	5.1	−0.525	−0.50			
26	29.8	5.8	−0.50	−0.475	9	36.4	12.1
19	21.7	4.9	−0.475	−0.45			
24	27.4	5.6	−0.45	−0.425	16	64.5	16.1
12	13.7	4.0	−0.425	−0.40			
18	20.6	4.9	−0.40	−0.375	9	36.3	12.1
20	22.9	5.1	−0.375	−0.35			
13	14.8	4.1	−0.35	−0.325	19	75.7	17.4
22	25.2	5.4	−0.325	−0.30			
17	19.5	4.7	−0.30	−0.275	6	24.0	9.7
16	18.3	4.6	−0.275	−0.25			
16	18.3	4.6	−0.25	−0.225	3	11.8	6.8
24	27.5	5.6	−0.225	−0.20			
21	24.1	5.3	−0.20	−0.175	6	24.0	9.8
20	22.8	5.1	−0.175	−0.15			
18	20.6	4.9	−0.15	−0.125	5	19.7	8.8
19	21.7	5.0	−0.125	−0.10			
14	16.0	4.3	−0.10	−0.075	5	19.7	8.8
27	30.9	5.9	−0.075	−0.05			
23	25.2	5.4	−0.05	−0.025	3	11.8	6.8
17	19.5	4.7	−0.025	−0.00			
18	20.6	4.9	0.00	0.025	3	13.1	7.6
18	20.6	4.9	0.025	0.05			
18	20.6	4.9	0.05	0.075	1	4.3	4.3
25	28.6	5.7	0.075	0.10			
19	21.7	5.0	0.10	0.125	2	8.8	6.2
23	26.3	5.5	0.125	0.15			
14	16.0	4.3	0.15	0.175	3	13.1	7.5
19	21.7	5.0	0.175	0.20			
17	19.4	4.7	0.20	0.225	3	12.9	7.4
23	26.3	5.5	0.225	0.25			
23	26.3	5.5	0.25	0.275	9	38.6	12.9
21	24.0	5.2	0.275	0.30			
19	21.7	5.0	0.30	0.325	11	47.1	14.2
33	37.8	6.6	0.325	0.35			
33	37.8	6.6	0.35	0.375	10	42.7	13.5
35	40.0	6.8	0.375	0.40			
35	40.0	6.8	0.40	0.425	14	60.2	16.1
39	44.6	7.1	0.425	0.45			
38	43.5	7.1	0.45	0.475	19	84.8	19.8
50	57.2	8.1	0.475	0.50			
58	66.4	8.7	0.50	0.525	12	51.2	14.8
62	70.9	9.0	0.525	0.55			
88	100.7	10.7	0.55	0.575	19	80.5	18.5
80	91.5	10.3	0.575	0.60			
80	89.2	10.1	0.60	0.625	15	64.1	16.6
113	125.6	12.0	0.625	0.65			
106	118.9	11.7	0.65	0.675	13	55.8	15.5
141	157.8	13.4	0.675	0.70			
133	148.7	13.0	0.70	0.725	18	75.9	17.9
160	178.4	14.3	0.725	0.75			

$K^-p \to K^-p$ Raw	Correct	Error	$\cos\theta_p$		$K^-p \to \bar{K}^0n$ Raw	Correct	Error
176	196.7	15.0	0.75	to 0.775	17	71.4	17.3
193	216.0	15.7	0.775	0.80			
229	256.1	17.1	0.80	0.825	11	46.2	13.9
273	305.3	18.7	0.825	0.85			
302	337.3	19.6	0.85	0.875	14	59.9	16.1
301	336.1	19.6	0.875	0.90			
372	417.2	21.8	0.90	0.925	21	87.9	19.2
356	469.9	25.3	0.925	0.95			
344	532.8	28.8	0.95	0.975	19	79.4	18.2
155	603.7	49.0	0.975	1.00			

$K^-p \to \Sigma^+\pi^-$ Raw	Correct	Error	$\cos\theta_p$		$K^-p \to \Sigma^-\pi^+$ Raw	Correct	Error
18	57.9	13.6	−1.00 to	−0.95	23	37.7	7.9
30	96.1	17.5	−0.95	−0.90	21	34.1	7.4
26	83.8	16.4	−0.90	−0.85	14	22.8	6.1
14	48.3	12.5	−0.85	−0.80	7	11.4	4.3
19	61.3	14.1	−0.80	−0.75	3	4.9	2.8
5	16.2	7.2	−0.75	−0.70	6	9.8	4.0
10	32.4	10.3	−0.70	−0.65	4	6.5	3.3
1	3.2	3.2	−0.65	−0.60	11	18.0	5.4
4	13.0	6.5	−0.60	−0.55	4	6.6	3.3
1	3.3	3.3	−0.55	−0.50	2	3.3	2.3
7	23.0	8.7	−0.50	−0.45	4	6.6	3.3
0	...	...	−0.45	−0.40	6	9.9	4.1
5	16.5	7.4	−0.40	−0.35	2	3.3	2.3
1	3.3	3.3	−0.35	−0.30	1	1.7	1.7
1	3.3	3.3	−0.30	−0.25	3	5.0	2.9
1	3.3	3.3	−0.25	−0.20	3	5.0	2.9
3	10.0	5.8	−0.20	−0.15	3	5.0	2.9
7	23.5	8.9	−0.15	−0.10	1	1.8	1.8
6	20.2	8.3	−0.10	−0.05	4	6.7	3.3
10	33.9	10.7	−0.05	−0.00	3	5.0	2.9
10	34.1	10.8	0.00	0.05	1	1.7	1.7
8	27.4	9.7	0.05	0.10	3	5.1	2.9
10	34.4	10.9	0.10	0.15	9	15.2	5.1
4	13.9	6.9	0.15	0.20	6	10.2	4.1
11	38.4	11.6	0.20	0.25	5	8.5	3.8
11	38.7	11.7	0.25	0.30	7	11.9	4.5
14	49.5	13.2	0.30	0.35	10	17.8	5.7
9	32.4	10.8	0.35	0.40	13	22.4	6.2
7	25.5	9.6	0.40	0.45	11	19.0	5.7
4	14.7	7.4	0.45	0.50	10	17.4	5.5
3	11.1	6.4	0.50	0.55	4	7.0	3.5
4	15.1	7.6	0.55	0.60	5	8.8	3.9
5	19.2	8.6	0.60	0.65	12	21.4	6.2
5	19.7	8.8	0.65	0.70	7	12.6	4.8
19	76.6	17.6	0.70	0.75	4	7.3	3.7
13	54.6	15.1	0.75	0.80	13	24.2	6.7
20	87.5	19.6	0.80	0.85	12	22.8	6.6
28	131.3	24.8	0.85	0.90	16	31.2	7.8
36	188.2	31.4	0.90	0.95	43	89.0	13.6
45	292.4	43.9	0.95	1.00	45	103.2	15.4

$K^-p \to \Lambda\pi^0$ Raw	Correct	Error			$K^-p \to \Xi^-K^+$ Raw	Correct	Error
9	35.6	11.9	−1.00 to	−0.95	0	...	...
11	42.6	12.8	−0.95	−0.90			
2	7.7	5.5	−0.90	−0.85	0	...	...
5	19.6	8.8	−0.85	−0.80			
5	19.5	8.7	−0.80	−0.75	0	...	...
5	19.7	8.8	−0.75	−0.70			
6	23.4	9.5	−0.70	−0.65	1	5.6	5.6
2	7.9	5.6	−0.65	−0.60			
6	23.6	9.6	−0.60	−0.55	1	5.4	5.4
3	11.7	6.8	−0.55	−0.50			
6	24.1	9.8	−0.50	−0.45	0	...	...
4	15.7	7.9	−0.45	−0.40			
3	11.8	6.8	−0.40	−0.35	1	5.4	5.4
1	3.9	3.9	−0.35	−0.30			

TABLE VI. (*continued*).

$K^-p \to \Lambda\pi^0$ Raw	Correct	Error			$K^-p \to \Xi^-K^+$ Raw	Correct	Error
2	8.2	5.8	−0.30	−0.25	0	...	...
2	7.8	5.5	−0.25	−0.20			
2	7.9	5.5	−0.20	−0.15	1	5.4	5.4
1	4.1	4.1	−0.15	−0.10			
1	4.0	4.0	−0.10	−0.05	3	16.3	9.4
2	7.9	5.6	−0.05	−0.00			
4	16.4	8.2	0.00	0.05	2	10.8	7.6
3	11.9	6.9	0.05	0.10			
4	16.3	8.1	0.10	0.15	1	5.4	5.4
7	27.8	10.5	0.15	0.20			
6	24.0	9.8	0.20	0.25	0	...	...
8	32.2	11.4	0.25	0.30			
11	44.8	13.5	0.30	0.35	0	...	...
11	46.8	14.3	0.35	0.40			
5	20.3	9.1	0.40	0.45	1	5.2	5.2
17	69.7	16.9	0.45	0.50			
15	62.1	16.0	0.50	0.55	1	5.2	5.2
16	65.5	16.4	0.55	0.60			
9	37.3	12.4	0.60	0.65	1	5.2	5.2
15	61.9	16.0	0.65	0.70			
13	54.2	15.0	0.70	0.75	4	20.4	10.2
12	52.5	15.3	0.75	0.80			
19	80.9	18.6	0.80	0.85	2	10.2	7.2
9	39.2	13.1	0.85	0.90			
9	41.3	13.8	0.90	0.95	0	...	...
10	50.9	16.1	0.95	1.00			

D. Angular Distributions

1. Production

As explained, the corrections of the raw data took into account the neutral particles that decayed outside the chamber (or indistinguishably near the vertex), pion contamination, scanning losses for small-angle scattering, and Dalitz pairs. Table VI presents the raw

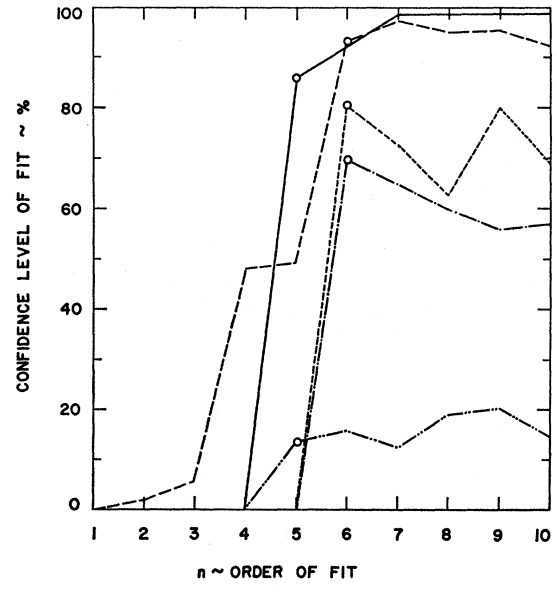

FIG. 7. Confidence level as a function of order of fit for the production angular distributions. — —, $\Lambda\pi^0$, 20 bins; ———, K^-p, 80 bins; – – – –, $\Sigma^-\pi^+$, 16 bins; —·—, $\bar{K}^0n$, 40 bins; and —··—, $\Sigma^+\pi^-$, 20 bins. Chosen order of best fit is indicated by a circle.

TABLE VII. Coefficients of production and decay angular distribution expansions.

Reaction	N	Normalization uncertainty	A_0	A_1	A_2	A	A_4	A_5	A_6	A_7	A_8
$K^-p \to K^-p$	5	3%	3.295 ±0.042	5.509 ±0.101	6.832 ±0.132	5.173 ±0.141	2.578 ±0.136	1.520 ±0.117	...	...	...
	6		3.293 ±0.041	5.463 ±0.101	6.767 ±0.133	5.009 ±0.155	2.371 ±0.159	1.296 ±0.147	−0.304 ±0.126	...	...
	7		3.293 ±0.039	5.474 ±0.095	6.841 ±0.129	5.118 ±0.150	2.621 ±0.168	1.604 ±0.167	0.013 ±0.151	0.422 ±0.127	...
$\to \bar{K}^0n$	6	10%	0.598 ±0.026	−0.126 ±0.056	0.864 ±0.072	−0.592 ±0.090	0.372 ±0.094	−0.580 ±0.088	0.721 ±0.100	...	...
	7		0.598 ±0.026	−0.130 ±0.058	0.868 ±0.074	−0.594 ±0.092	0.376 ±0.100	−0.594 ±0.106	0.726 ±0.104	−0.013 ±0.108	...
	8		0.598 ±0.028	−0.130 ±0.060	0.868 ±0.078	−0.598 ±0.096	0.378 ±0.102	−0.596 ±0.112	0.732 ±0.122	−0.013 ±0.110	0.012 ±2.10
$\to \Sigma^+\pi^-$	5	10%	0.248 ±0.015	0.212 ±0.037	0.496 ±0.049	0.222 ±0.054	0.416 ±0.047	0.268 ±0.048	...	...	...
	6		0.248 ±0.015	0.220 ±0.037	0.511 ±0.051	0.235 ±0.055	0.454 ±0.061	0.285 ±0.051	0.064 ±0.059	...	...
	7		0.248 ±0.016	0.217 ±0.039	0.505 ±0.055	0.223 ±0.064	0.449 ±0.065	0.263 ±0.074	0.055 ±0.063	−0.026 ±0.060	...
$\to \Sigma^-\pi^+$	6	6%	0.064 ±0.003	0.053 ±0.006	0.122 ±0.009	0.044 ±0.010	0.107 ±0.011	0.061 ±0.010	0.076 ±0.011	...	...
	7		0.064 ±0.003	0.053 ±0.007	0.122 ±0.010	0.043 ±0.012	0.107 ±0.012	0.060 ±0.014	0.076 ±0.012	−0.001 ±0.013	...
	8		0.064 ±0.003	0.053 ±0.008	0.123 ±0.011	0.044 ±0.013	0.108 ±0.016	0.060 ±0.016	0.077 ±0.018	−0.001 ±0.014	0.002 ±0.016
$\to \Lambda\pi^0$	5	12%	0.188 ±0.012	0.163 ±0.023	0.133 ±0.028	−0.113 ±0.036	−0.128 ±0.038	−0.043 ±0.041	...	...	...
	6		0.188 ±0.008	0.152 ±0.016	0.131 ±0.019	−0.121 ±0.025	−0.077 ±0.029	−0.011 ±0.029	0.116 ±0.032	...	...
	7		0.188 ±0.007	0.145 ±0.015	0.133 ±0.017	−0.125 ±0.022	−0.074 ±0.025	−0.042 ±0.029	0.095 ±0.029	−0.065 ±0.032	...

Reaction	M	Normalization uncertainty	B_1	B_2	B_3	B_4	B_5	B_6	B_7	Confidence level
$K^-p \to \Lambda\pi^0$	5	12%	−0.0136 ±0.0268	+0.0290 ±0.0330	−0.0081 ±0.0178	−0.0063 ±0.0154	+0.0092 ±0.0134	...	...	9.89
	6		−0.0123 ±0.0266	+0.0314 ±0.0229	−0.0045 ±0.0179	−0.0115 ±0.0160	+0.0045 ±0.0140	−0.0121 ±0.0115	...	14.73
	7		−0.0095 ±0.0296	+0.0298 ±0.0254	−0.0064 ±0.0199	−0.0133 ±0.0178	+0.0073 ±0.0160	−0.076 ±0.0143	+0.0089 ±0.0131	13.82
$\to \Sigma^+(p)\pi^-$	5	10%	−0.0134 ±0.0252	+0.0384 ±0.0233	+0.0569 ±0.0246	+0.0555 ±0.0185	+0.0160 ±0.0169	...	...	22.86
	6		−0.0243 ±0.0233	+0.0249 ±0.0224	+0.0523 ±0.0218	+0.0384 ±0.0199	+0.0108 ±0.0153	−0.0196 ±0.0132	...	40.96
	7		−0.0261 ±0.0121	+0.0168 ±0.0119	+0.0386 ±0.0121	+0.0316 ±0.0105	−0.0056 ±0.0096	−0.0281 ±0.0074	−0.0206 ±0.0068	87.14

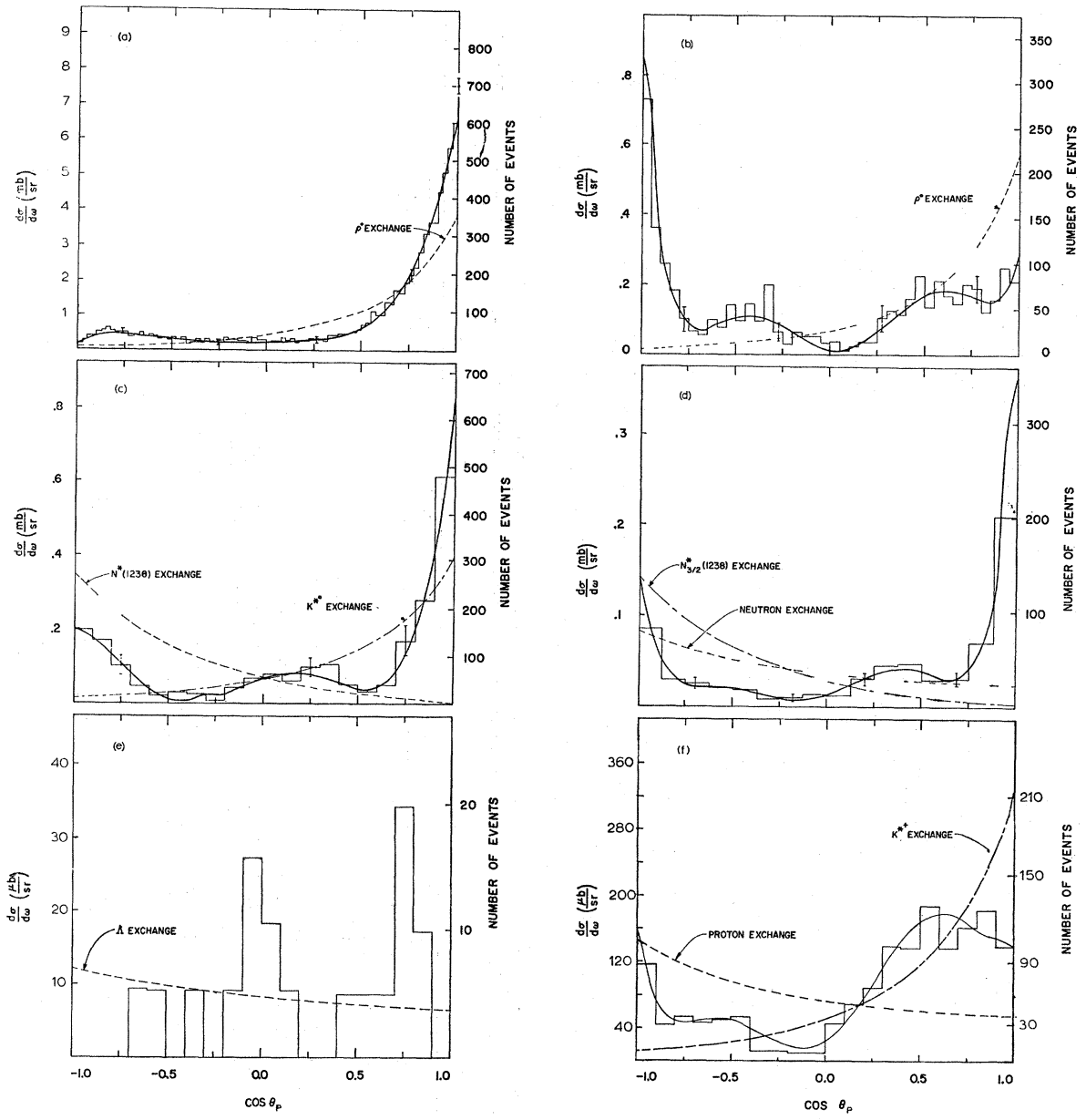

FIG. 8. Production angular distribution. (a) $K^-p \to K^-p$ fitted to $n=5$ and with ρ^0 exchange; (b) $K^-p \to \bar{K}^0 n$ fitted to $n=6$ and with ρ^+ exchange; (c) $K^-p \to \Sigma^+\pi^-$ fitted to $n=5$ and with K^{*0} (891) and $N_{3/2}{}^{*++}$ (1238) exchange; (d) $K^-p \to \Sigma^-\pi^+$ fitted to $n=6$ and with n and $N_{3/2}{}^{*0}$ (1238) exchange; (e) $K^-p \to \Xi^-K^+$ not fitted with Legendre series, but with Λ exchange; (f) $K^-p \to \Lambda\pi^0$ fitted to $n=6$ and p and K^{*+} (891) exchange.

and corrected production angular distributions and their errors. The magnitude of each bin and its error are given by

$$Y \pm \Delta Y = \sum_{i=1}^{I} Y_i{}^c \pm [\sum_{i=1}^{I} (y_i{}^c)^2]^{1/2}, \qquad (13)$$

where $y_i{}^c$ is the weight of the ith event after the corrections are applied. The production cosine interval for which the corrected number of events is being calculated contains I raw events.

Each adjusted-production angular distribution was fitted by the least-square criterion to a series of the form

$$Y = \frac{\tau}{k^2} \sum_{n=0}^{N} A_n P_n(\cos\theta_P), \qquad (14)$$

where $P_n(\cos\theta_P)$ is the Legendre polynomial of order n, and k is the incident-kaon wave number. The isotopic spin factor τ is the square of the multiplicative constant

in each of the isotopic spin amplitudes;

$$\begin{aligned} T_{K^-p}&=\tfrac{1}{2}(T^0+T^1),\\ T_{\bar{K}^0n}&=\tfrac{1}{2}(T^0-T^1),\\ T_{\Sigma^+\pi^-}&=\tfrac{1}{2}\sqrt{2}(N^0/\sqrt{3}-N^1/\sqrt{2}),\\ T_{\Sigma^-\pi^+}&=\tfrac{1}{2}\sqrt{2}(N^0/\sqrt{3}+N^1/\sqrt{2}),\\ T_{\Sigma^0\pi^0}&=\tfrac{1}{2}\sqrt{2}N^0/\sqrt{3},\\ T_{\Lambda\pi^0}&=\tfrac{1}{2}\sqrt{2}M^1. \end{aligned} \tag{15}$$

The component isotopic spin amplitude for each process which appears on the left of these equations is superscripted with the appropriate isospin designation. The determination of the order n of the best fit was made by applying the χ^2 test to fits made to the data with different bin sizes. For the optimum bin size, the confidence levels of the fits to each measured reaction are plotted as a function of n in Fig. 7. The n chosen by the above procedure is indicated by a circle. Its appropriateness has been corroborated by applying the Fisher F test.[15]

For the elastic scattering differential cross section, the forward scattering amplitude can be written as

$$\left(\frac{d\sigma}{d\omega}\right)_{\theta=0^0}=|\mathrm{Im}f(\theta)|^2_{\theta=0^0}+|\mathrm{Re}f(\theta)|^2_{\theta=0^0}. \tag{16}$$

By the optical theorem,

$$|\mathrm{Im}f(\theta)|^2_{\theta=0^0}=[(k/4\pi)\sigma_{\mathrm{tot}}]^2=(6.29\pm0.16)\ \mathrm{mb/sr} \tag{17}$$

and by dispersion relations,[16]

$$|\mathrm{Re}f(\theta)|^2_{\theta=0^0}=0.055\pm0.15\ \mathrm{mb/sr}.$$

The fit to the elastic production angular distributions was not constrained by the value predicted by the optical theorem.

Table VII presents the coefficients from the three best fits for each distribution. The normalization for each of the sets of fitted coefficients was made so that

$$A_0=\sigma_{\mathrm{partial}}/4\pi\lambda^2\tau.$$

TABLE VIII. Polarization distributions for $K^-p\to\Lambda\pi^0$ and $\Sigma^+(p)\pi^-$.

$K^-p\to\Lambda\pi^0$ $\langle\alpha P\rangle$	Error	$\cos\theta_p$		$K^-p\to\Sigma^+(p)\pi^-$ $\langle\alpha P\rangle$	Error
+0.33	0.33	−1.00 to	−0.80	+0.01	0.24
−1.22	0.29	−0.80	−0.60	−0.20	0.34
−0.03	0.40	−0.60	−0.40	−0.26	0.70
−1.02	0.50	−0.40	−0.20	+0.17	0.70
−0.11	0.71	−0.20	−0.00	−0.16	0.43
+0.06	0.41	0.00	0.20	−0.59	0.33
+0.29	0.29	0.20	0.40	−0.84	0.25
−0.05	0.24	0.40	0.60	−0.52	0.38
+0.20	0.25	0.60	0.80	+0.94	0.28
−0.07	0.25	0.80	1.00	+0.02	0.18

[15] R. A. Fisher, *Statistical Methods for Research Workers* (Hafner Publishing Co., New York, 1946), 10th ed., Table IV, p. 174.

[16] V. Cook, D. Keefe, L. T. Kerth, P. G. Murphy, W. A. Wenzel, and T. F. Zipf, Phys. Rev. **129**, 2743 (1963).

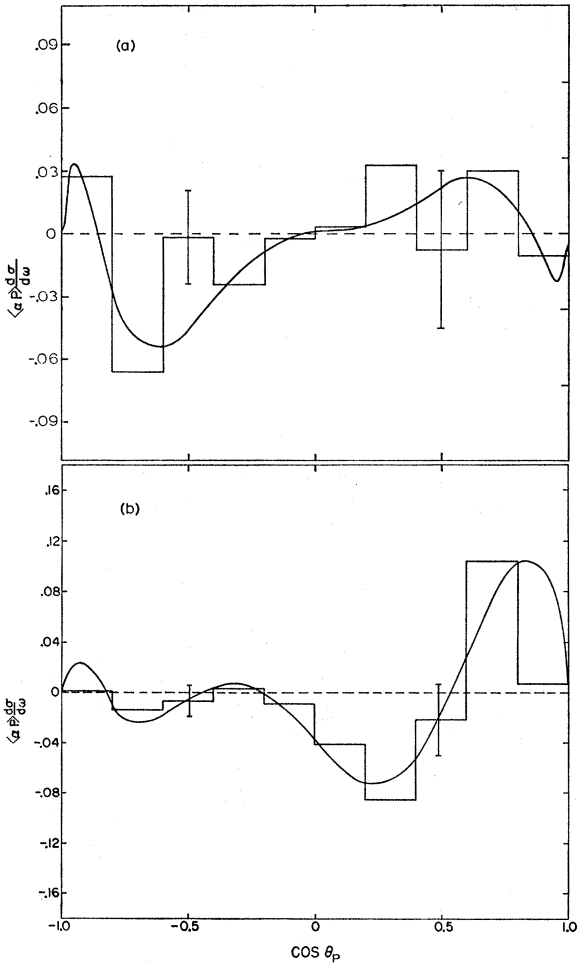

FIG. 9. Decay angular distribution. (a) $K^-P\to\Lambda(\mathrm{lo})\pi^0$ and then $\Lambda\to p\pi^-$ fit to $m=6$. (b) $K^-p\to\Sigma^+(p)\pi^-$ and then $\Sigma^+(p)\to p\pi^0$ fit to $m=6$.

Figures 8(a)–8(f) display the weighted angular distributions and their best fitted curves. Figure 8(e) shows the weighted $K^-p\to\Xi^-K^+$ distribution which was not fitted because of the small number of events.

2. Polarization

It is well known that the Λ and $\Sigma^+(p)$ both have large decay asymmetry parameters, usually called α.[17] To determine the polarization involved in the production process, the orientation with respect to the production plane of the decay-product proton was calculated by

$$\cos\psi=\frac{\mathbf{P}_{K^-}\times\mathbf{P}_{\mathrm{hyperon}}}{|\mathbf{P}_{K^-}\times\mathbf{P}_{\mathrm{hyperon}}|}\cdot\hat{p}_p. \tag{18}$$

A histogram of this quantity, given in Table VIII was

[17] A. H. Rosenfeld, A. Barbaro-Galtieri, W. J. Podolsky, L. R. Price, P. Soding, M. Roos, C. G. Wohl, and W. S. Willis, Rev. Mod. Phys. **39**, 1 (1967).

TABLE IX. Average polarization for some two-body decays.

Reaction	Decay[a] asymmetry α	Number of events	$3\Sigma \cos\Psi$	$\langle \alpha P \rangle$	P
$K^- p \to \bar{K}^0 n$	0	490	+14.0	+0.03±0.06	...
$\to \Sigma^+(n)\pi^-$	+0.008±0.037	437	−26.6	−0.06±0.03	−7.5 ±34.7
$\to \Sigma^+(p)\pi^-$	−0.960±0.067	312	−34.1	−0.11±0.03	+0.11±0.04
$\to \Sigma^-(n)\pi^+$	−0.010±0.043	361	−65.2	−0.18±0.03	+18.0 ±77.5
$\to \Lambda\pi^0$	−0.663±0.022	281	−6.35	−0.02±0.03	+0.03±0.05

[a] See Ref. 11.

constructed by

$$Y=\langle \alpha P \rangle = \frac{3}{I}\sum_{i=1}^{I} \cos\psi_i \tag{19}$$

and

$$\Delta Y = [(3-\langle \alpha P \rangle^2)/I]^{1/2}, \tag{20}$$

where P is the average polarization in an interval of $\cos\theta_P$. These distributions were then fitted to

$$\langle \alpha P \rangle \frac{d\sigma}{d\omega} = \frac{1}{4\pi k^2 \tau} \sum_{m=1}^{M} B_m P_m^1(\cos\theta_P), \tag{21}$$

where $P_m^1(\cos\theta_P)$ are the usual[18] first-associated Legendre polynomials of order m. The order of best fit, chosen on the basis of its confidence level, was again tested by the Fisher F test.

Table VII presents the coefficients from the three best fits to the distributions. Figures 9(a) and 9(b) display the polarization angular distributions for $\Lambda(1o)\pi^0$ and $\Sigma^+(p)\pi^-$, respectively, together with the curve that best fit the data.

The average polarization was calculated for each two-body reaction for which the production distribution was measured. Since only the $\Sigma^+(p)$ and Λ have sizable decay asymmetries, the values obtained from the other final states are included only to indicate the reliability of these measurements. The results are tabulated in Table IX. The value of $\langle \alpha P \rangle$ that we find for the $\Sigma^-(n)\pi^+$ final state is much larger than the largest possible value, $\langle \alpha P \rangle_{\max} = \langle \alpha \rangle = 0.010 \pm 0.043$, found elsewhere.[17] However, we have investigated the $\Sigma^-(n)\pi^+$ final state thoroughly and have found no apparent biases. All other final states listed have values of $\langle \alpha P \rangle$ compatible with α within the statistical uncertainties.

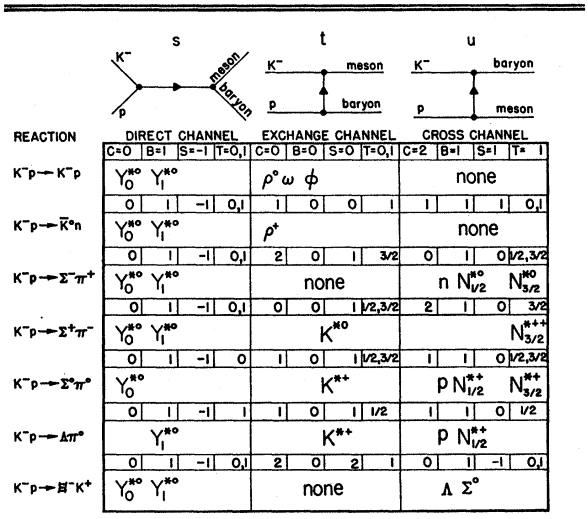

REACTION	DIRECT CHANNEL C=0 B=1 S=−1 T=0,1	EXCHANGE CHANNEL C=0 B=0 S=0 T=0,1	CROSS CHANNEL C=2 B=1 S=1 T=1
$K^-p \to K^-p$	Y_0^{*0} Y_1^{*0}	$\rho^0 \omega \phi$	none
	0 1 −1 0,1	1 0 0 1	1 1 1 0,1
$K^-p \to \bar{K}^0 n$	Y_0^{*0} Y_1^{*0}	ρ^+	none
	0 1 −1 0,1	2 0 1 3/2	0 1 0 1/2,3/2
$K^-p \to \Sigma^-\pi^+$	Y_0^{*0} Y_1^{*0}	none	n $N_{1/2}^{*0}$ $N_{3/2}^{*0}$
	0 1 −1 0,1	0 0 1 1/2,3/2	2 1 0 3/2
$K^-p \to \Sigma^+\pi^-$	Y_0^{*0} Y_1^{*0}	K^{*0}	$N_{3/2}^{*++}$
	0 1 −1 0	1 0 1 1/2,3/2	1 1 0 1/2,3/2
$K^-p \to \Sigma^0\pi^0$	Y_0^{*0}	K^{*+}	p $N_{1/2}^{*+}$ $N_{3/2}^{*+}$
	0 1 −1 1	1 0 1 1/2	1 1 0 1/2
$K^-p \to \Lambda\pi^0$	Y_1^{*0}	K^{*+}	p $N_{1/2}^{*+}$
	0 1 −1 0,1	2 0 2 1	0 1 −1 0,1
$K^-p \to \Xi^-K^+$	Y_0^{*0} Y_1^{*0}	none	Λ Σ^0

FIG. 10. Exchange candidates for some two-body reactions. C is the charge, B is the baryon number, S is the strangeness, and T is the isotopic spin of the candidate.

[18] The sign convention used is that of J. D. Jackson, *Classical Electrodynamics* (John Wiley & Sons, Inc., New York, 1962), p. 65.

IV. DISCUSSION OF RESULTS

A. Comparison with Simple Feynman Graphs

The three simplest Feynman graphs that describe the reactions we have measured are shown in Fig. 10. Also shown are the particles that can act as propagators

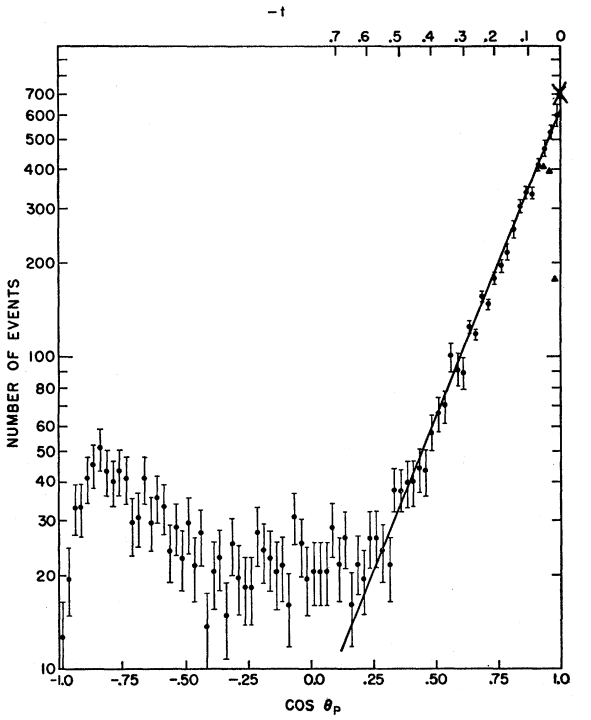

FIG. 11. Semilogarithmic plot of elastic scattering production angular distribution. The first three bins also display data not corrected for short unseen proton events (▲). The optical point is indicated (✕).

in the three diagrams of the various reactions. The production angular distributions that would be predicted by assuming any one of the possible propagators of the t and u channels were calculated. None of them was representative of the observed data. They are shown in Figs. 8(a)–8(f).

The s channel remains as a possibility. From the order of Legendre polynomial required to fit the production angular distributions,[19] it can be inferred that an intermediate state of spin $\frac{5}{2}$ was involved in the K^-p and $\Sigma^+\pi^-$ final states. An intermediate state of spin $\frac{7}{2}$ is inferred for $\bar{K}^0n$, $\Sigma^-\pi^+$, and $\Lambda\pi^0$ production. From the fits to the angular dependence of the polarization, it is inferred that an intermediate state of spin $\frac{7}{2}$ is involved in the $\Sigma^+\pi^-$ and $\Lambda\pi^0$ final states. The possibility of propitious cancellation could cause the disagreement in the results for the $\Sigma^+\pi^-$ final state.

B. Comparison of Elastic Scattering with an Optical Model

Viewing the elastic scattering as a diffraction process, we use the forward portion of our measured elastic scattering production angular distributions and the total cross section to obtain the parameters of a specific optical model. For the derivation of this model we refer to the work of Krisch,[20] in which it is assumed that the elastic reaction is dominated by spin-independent absorptive processes. The scatterer is taken to be a grey disk of radius R with a transmission coefficient e^{-A}. A partial-wave analysis is performed in which the phase shift and absorption coefficient for each partial wave is taken to be independent of l for $0<l\leq kR$ and to vanish for $l>kR$.

This model then predicts that for c.m. production angles of up to about 70°, the elastic production angular distribution should be

$$\frac{d\sigma}{d\omega}\propto\left[\frac{J_1(2kR\sin\frac{1}{2}\theta_P)}{kR\sin\frac{1}{2}\theta_P}\right]^2. \tag{22}$$

The optical theorem predicts, for this model, a total cross section of

$$\sigma_{\text{tot}}=2\pi R^2(1-e^{-A}). \tag{23}$$

Kirsch further points out that Eq. (22) can be approximated by

$$d\sigma/d\omega\propto\exp[-k^2R^2\sin^2(\tfrac{1}{2}\theta_P)]\propto\exp(\tfrac{1}{4}R^2t) \tag{24}$$

which is good to better than 10% for c.m. production angles less than 70°. The quantity t is the square of the four-momentum transfer.

The semilog plot in Fig. 11 shows the number of elastic-scattering events in bins of equal t. The straight line was fitted to the data on the interval $0.67>-t\geq 0.061$. The fit gives a value of $R=0.94\pm0.04$ F. It is interesting to note that the observed distribution follows this prediction well out to $-t=0.6$ or $\theta_P=75°$.

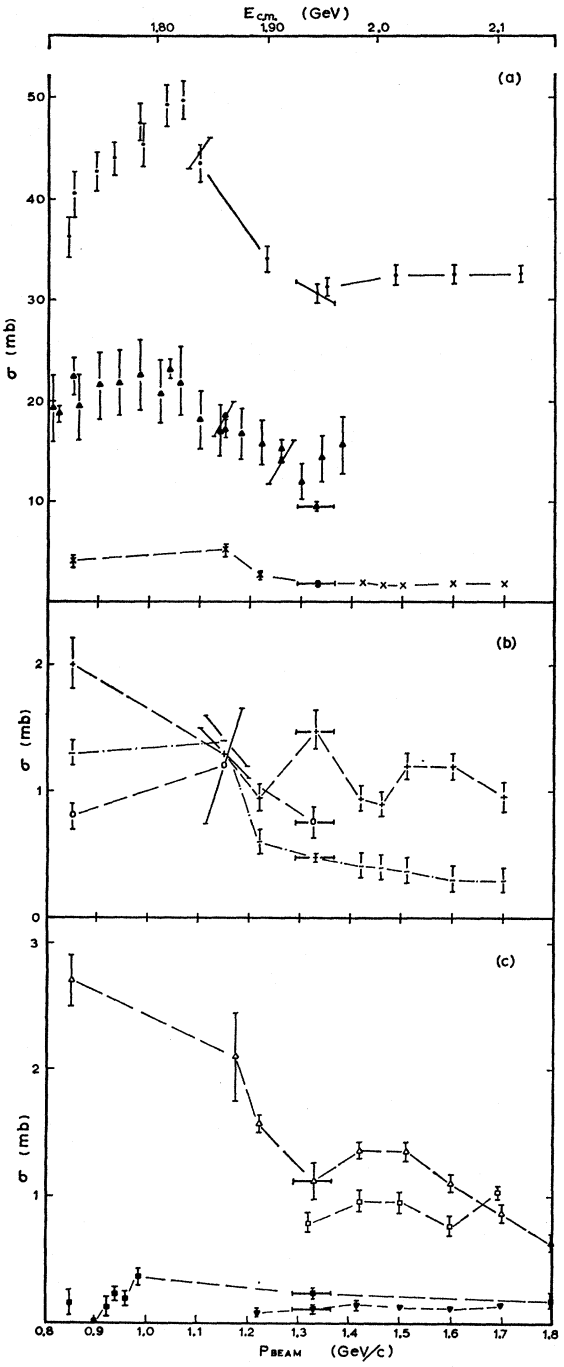

FIG. 12. Measured beam cross sections for momenta between 0.8 and 1.8 GeV/c. Our data are indicated at 1.33 GeV/c. (a) ● total; Refs. 2(a), 2(b), and 2(c). ▲ elastic; Refs. 2(c), 2(d), 3(a), and 3(b). × charge exchange; Refs. 2(c), 2(d), 3(c), and 3(d). (b) + $\Sigma^+\pi^-$; Refs. 2(c), 2(d), 3(e), and 3(f). − $\Sigma^-\pi^+$; Refs. 2(c), 2(d), 3(e), and 3(f). ○ $\Sigma^0\pi^0$; Refs. 2(c) and 2(d). (c) □ $\Lambda\omega$; Ref. 3(h). ■ $\Lambda\eta$; Refs. 2(c), 3(i), and 3(j). △ $\Lambda\pi^0$; Refs. 2(c), 2(d), 3(c), and 3(g). ▼ Ξ^-K^+; Ref. 3(k).

[19] L. E. Olson and W. P. Trower, J. Nat. Sci. Math. 4, 127 (1966).

[20] A. D. Krisch, *Lectures in Theoretical Physics* (University of Colorado Press, Boulder, 1965), Vol. VII-B, p. 249.

By use of this value of R and Eq. (23) the value of the transmission coefficient e^{-A} is found to be 0.45 ± 0.03.

Finally, when this fitted curve is extrapolated to $\cos\theta_P=+1.0$, an estimate for the real part of the forward scattering amplitude can be made from Eq. (16) to be

$$|\mathrm{Re}f(\theta)|^2_{\theta=0}=-0.54\pm0.53$$

and is consistent with zero. This implies that the phase shifts are purely imaginary.

C. Comparison of Results with Other Experiments

Figure 12 shows the total and partial two-body final state cross sections over the incident-kaon momentum interval 0.8–1.8 GeV/c. As can be seen, there is good agreement between our data and those of other authors. The expansion coefficients A_n and B_m for the various final states analyzed were also found to be consistent with the data of other authors. The single exception to this statement is the data for A_{1-6} in the $\Sigma^+\pi^-$ final state. Our results are somewhat larger than the other data at nearby energies.[2]

ACKNOWLEDGMENTS

The measuring equipment and film used in this experiment were obtained in collaboration with the Alvarez group of the Lawrence Radiation Laboratory, and the authors gratefully acknowledge the privilege of participating in this collaboration. Discussions with Professor R. L. Schult and Dr. J. T. Donohue regarding the calculations were very helpful. Professor E. L. Goldwasser's assistance during the preparation of the text is warmly appreciated.